Journal of Computational Physics **158,** 51–70 (2000)
doi:10.1006/jcph.1999.6406, available online at http://www.idealibrary.com on IDEAL®

Compact Implicit MacCormack-Type Schemes with High Accuracy

R. Hixon* and E. Turkel*,†

**Institute for Computational Mechanics in Propulsion (ICOMP), NASA Glenn Research Center, Cleveland, Ohio 44135; and †Tel Aviv University, Tel Aviv, Israel*
E-mail: fshixon@apu.grc.nasa.gov

Received April 19, 1999; revised November 2, 1999

In this work, the MacCormack methodology is extended to implicit compact differencing schemes. A prefactorization method is developed which splits the implicit matrix into two independent upper and lower matrices which are easier to invert. Using this method, a new class of high-order accurate compact MacCormack-type schemes is derived. Two fourth-order schemes are described, and results are shown for three linear and nonlinear CAA benchmark problems.

Key Words: MacCormack-type scheme; compact differencing.

1. INTRODUCTION

In aeroacoustic calculations, the propagation of unsteady flow and acoustic phenomena need to be accurately determined over long periods of time. To reduce the accumulation of error, the numerical spatial derivatives of the flow must be highly accurate while requiring few grid points to resolve each wave. To accomplish this goal, high-order and optimized finite-difference schemes have been developed (e.g., Refs. [1–11]).

There are two main classes of high-accuracy finite-difference schemes: explicit schemes and compact schemes. Explicit schemes directly compute the numerical derivative by employing large computational stencils for accuracy. Compact schemes use smaller stencils by solving a matrix for the numerical derivatives along a grid line. Thus, unlike an explicit scheme, the numerical derivative at each point depends on the value of the numerical derivative at neighboring points. While compact schemes are more accurate than the explicit scheme of the same order, solving for each spatial derivative requires a scalar tridiagonal or pentadiagonal matrix inversion.

Recently, a new class of high-accuracy explicit MacCormack-type schemes has been introduced for computational aeroacoustics [9, 10]. We extend this methodology to compact

0021-9991/00 $35.00

schemes, resulting in a class of highly accurate compact MacCormack-type schemes which use one-sided implicit stencils.

2. MATHEMATICAL FORMULATION

A general compact spatial derivative of a function f may be written as

$$[B]\{D\} = \frac{1}{\Delta x}[C]\{f\}, \tag{1}$$

where D is the numerical approximation to the spatial derivative of the function f, $[C]$ is the matrix of explicit coefficients, and $[B]$ is the matrix of implicit coefficients and must be inverted to obtain D.

For example, a fourth-order accurate approximation to the derivative is given by

$$\frac{1}{6}(D_{i+1} + 4D_i + D_{i-1}) = \frac{1}{2\Delta x}(f_{i+1} - f_{i-1}). \tag{2}$$

Since the value of D at a given point depends on the values of D at neighboring points, a scalar tridiagonal matrix must be solved to obtain the derivative:

$$\{D\} = [B]^{-1}\left(\frac{1}{\Delta x}[C]\{f\}\right). \tag{3}$$

In a MacCormack-type scheme, the derivative operator is split into forward and backward operators such that

$$\{D\} = \frac{\{D^F\} + \{D^B\}}{2}. \tag{4}$$

D^F and D^B use one-sided forward and backward differences, respectively. A Taylor series expansion yields

$$\begin{aligned} D^F &= f_x + Af_{xx} - Bf_{xxxx} - \cdots + O(\Delta x)^n \\ D^B &= f_x - Af_{xx} + Bf_{xxxx} + \cdots + O(\Delta x)^n. \end{aligned} \tag{5}$$

Extending the MacCormack concept to implicit operators, the derivative operators are defined as

$$\begin{aligned} [B^F]\{D^F\} &= \frac{1}{\Delta x}[C^F]\{f\} \\ [B^B]\{D^B\} &= \frac{1}{\Delta x}[C^B]\{f\} \end{aligned} \tag{6}$$

or

$$\begin{aligned} \{D^F\} &= [B^F]^{-1}\left(\frac{1}{\Delta x}[C^F]\{f\}\right) \\ \{D^B\} &= [B^B]^{-1}\left(\frac{1}{\Delta x}[C^B]\{f\}\right), \end{aligned} \tag{7}$$

where

$$[B^F] = [B^B]^T$$
$$[C^F] = -[C^B]^T. \tag{8}$$

Substituting into Eq. (3), we obtain

$$\{D\} = \frac{1}{2\Delta x}([B^F]^{-1}[C^F] + [B^B]^{-1}[C^B])\{f\}. \tag{9}$$

Using Eq. (8), this becomes

$$\{D\} = \frac{1}{2\Delta x}(-([B^B]^T)^{-1}[C^B]^T + [B^B]^{-1}[C^B])\{f\}. \tag{10}$$

Multiplying through and rearranging, we obtain

$$[B^B]^T[B^B]\{D\} = \frac{1}{2\Delta x}(-[B^B][C^B]^T + [B^B]^T[C^B])\{f\}. \tag{11}$$

Notice that Eq. (11) is only valid if

$$[B^B]^T[B^B] = [B^B][B^B]^T. \tag{12}$$

Equation (12) is true in the interior for all tridiagonal matrices with constant diagonals.

To avoid a tridiagonal matrix inversion, we use bidiagonal matrices for the forward and backward operators. Writing out the backward operator explicitly, we have

$$aD^B_{i-1} + (1-a-c)D^B_i + cD^B_{i+1} = \left(\frac{1}{\Delta x}\right)(kf_{i-1} - (k+m)f_i + mf_{i+1}). \tag{13}$$

Using the definitions of Eq. (8), the forward operator becomes

$$cD^F_{i-1} + (1-a-c)D^F_i + aD^F_{i+1} = \left(\frac{1}{\Delta x}\right)(-mf_{i-1} + (k+m)f_i - kf_{i+1}). \tag{14}$$

Using this, we find that at point i in the interior

$$\begin{aligned}[B^B]^T[B^B]\{D\}_i = {} & ca(D_{i-2} + D_{i+2}) + (c+a)(1-a-c)(D_{i-1} + D_{i+1}) \\ & + (c^2 + a^2 + (1-a-c)^2)D_i.\end{aligned} \tag{15}$$

Matching the coefficients in Eq. (15) with those on the left side of Eq. (2) gives

$$c = 0$$
$$a = \frac{1}{2} \pm \frac{1}{2\sqrt{3}}. \tag{16}$$

Here we take a to be the smaller of the two possible values. On the explicit side, we find

$$\begin{aligned}&\frac{1}{2\Delta x}(-[B^B][C^B]^T + [B^B]^T[C^B])\{f\}_i \\ &= \frac{1}{2\Delta x}((ma-kc)(f_{i+2} - f_{i-2}) + ((k+m)(c-a) + (1-a-c)(m-k))(f_{i+1} - f_{i-1})).\end{aligned} \tag{17}$$

Matching the coefficients in Eq. (17) with Eq. (2) gives

$$\begin{aligned} c &= 0 \\ m &= 0 \\ k &= -1 \end{aligned} \tag{18}$$

and thus

$$\begin{aligned} a D^B_{i-1} + (1-a) D^B_i &= \left(\frac{1}{\Delta x}\right)(f_i - f_{i-1}) \\ a D^F_{i+1} + (1-a) D^F_i &= \left(\frac{1}{\Delta x}\right)(f_{i+1} - f_i). \end{aligned} \tag{19}$$

Performing a Taylor series expansion of the forward and backward operators gives

$$\begin{aligned} D^F &= f_x + \Delta x \frac{\sqrt{3}}{6} f_{xx} - (\Delta x)^3 \frac{\sqrt{3}}{72} f_{xxxx} + O(\Delta x)^4 \\ D^B &= f_x - \Delta x \frac{\sqrt{3}}{6} f_{xx} + (\Delta x)^3 \frac{\sqrt{3}}{72} f_{xxxx} + O(\Delta x)^4. \end{aligned} \tag{20}$$

Two things can be seen in Eq. (20). First, the form of the two operators is similar to Eq. (5) in that the even derivatives are equal and opposite. Second, a fourth-order accurate central difference is recovered when the forward and backward operators are substituted into Eq. (4). Thus, the operators that have been defined are suitable for use in a MacCormack-type scheme. Unlike the work by Kennedy *et al.* [8], which derived compact MacCormack-type operators with tridiagonal matrices, the operator is one-sided on the implicit side as well. Using the terminology of Hixon [9], this method is a 4/2 scheme. This terminology refers to the order of the underlying fourth-order central difference and the leading error term in the first-order biased differences. It should be noted, however, that the prefactorization method is not limited to MacCormack-type schemes; other work has used this prefactorization method to obtain more efficient central difference compact derivatives [11] and compact filters [12].

Notice that since bidiagonal matrices are used to calculate the derivatives, the local value of D may be found using the value of D on one side only. By sweeping in the proper direction, the values of D may be found explicitly.

By using an additional explicit point and following the method used in Ref. [9], the order of the forward and backward operators may be increased to third order, resulting in a 4/4 scheme. This scheme is defined by

$$\begin{aligned} a &= \frac{1}{3} \\ m &= \frac{1}{6} \\ k &= -\frac{5}{6} \end{aligned} \tag{21}$$

and thus

$$\frac{1}{3}D^B_{i-1} + \frac{2}{3}D^B_i = \left(\frac{1}{\Delta x}\right)\left(\frac{1}{6}f_{i+1} + \frac{2}{3}f_i - \frac{5}{6}f_{i-1}\right)$$
$$\frac{1}{3}D^F_{i+1} + \frac{2}{3}D^F_i = \left(\frac{1}{\Delta x}\right)\left(\frac{5}{6}f_{i+1} - \frac{2}{3}f_i - \frac{1}{6}f_{i-1}\right). \tag{22}$$

Consequently, one extra point is used in the explicit operator to achieve the increase in order. The Taylor series expansion of the forward and backward operators is

$$D^F = F_x - (\Delta x)^3\frac{1}{36}F_{xxxx} + O(\Delta x)^4$$
$$D^B = F_x + (\Delta x)^3\frac{1}{36}F_{xxxx} + O(\Delta x)^4. \tag{23}$$

Substituting the coefficients of Eq. (21) into Eqs. (15) and (17) reveals that the 4/4 scheme reduces to the following fourth-order compact central difference:

$$\frac{2}{9}D_{i-1} + \frac{5}{9}D_i + \frac{2}{9}D_{i+1} = \left(\frac{1}{\Delta x}\right)\left(\frac{1}{36}F_{i+2} + \frac{4}{9}F_{i+1} - \frac{4}{9}F_{i-1} - \frac{1}{36}F_{i-2}\right). \tag{24}$$

This illustrates one very important difference between the explicit MacCormack-type schemes given in Ref. [9] and the compact MacCormack-type schemes described here. For explicit schemes, the order of the forward and backward operators may be changed without changing the underlying central difference. Thus, the sum of the forward and backward operators for the explicit 4/2 and 4/4 schemes is the same fourth-order central difference, giving identical dispersion properties. However, the compact 4/2 and 4/4 schemes have different underlying central differences, which give completely different dispersion properties, as will be illustrated.

Notice that using a larger stencil on the forward and backward operators results in a larger equivalent stencil for the underlying difference. As shown in Ref. [11], this method can be used to derive a class of prefactored small-stencil high-order compact central differences.

Table I gives a comparison of the computational work required to compute a derivative using the 4/2 or 4/4 scheme. From this comparison, the compact MacCormack-type schemes are very competitive with explicit central differences as well as with compact central differences.

TABLE I
Work per Point Comparison

Scheme	Multiplies	Additions
4/2	2	2
4/4	3	4
Explicit 4	2	3
Explicit 6	3	4
7-point DRP	3	4
Compact 4	3	3

3. TIME MARCHING METHODS

Given the equation

$$U_t + \{F(U)\}_x = 0 \tag{25}$$

the original MacCormack scheme used a two-stage explicit time marching method:

$$\begin{aligned} U^{(1)} &= U^n - \Delta t \delta^F [F(U^n)] \\ U^{n+1} &= \frac{1}{2}\left(U^n + U^{(1)} - \Delta t \delta^B \left[F\left(U^{(1)}\right)\right]\right). \end{aligned} \tag{26}$$

This scheme is second-order accurate in time, and fourth-order accurate in space using the 4/2 compact-implicit scheme given in Eqs. (16) and (18) for linear problems. To obtain fourth-order accuracy in space for nonlinear problems, one needs to permute the forward and backward differences (see Ref. [2]).

In addition to a MacCormack two-stage scheme, three multistage Runge–Kutta-type time marching methods for MacCormack-type schemes will be described. These methods were derived for MacCormack-type schemes in Ref. [9] and will be briefly described here.

A general six-stage Runge–Kutta MacCormack-type scheme can be defined as

$$\begin{aligned} h^{(1)} &= -\Delta t \delta^F [F(U^n)] \\ h^{(2)} &= -\Delta t \delta^B \left[F\left(U^n + \alpha_2 h^{(1)}\right)\right] \\ h^{(3)} &= -\Delta t \delta^F \left[F\left(U^n + \alpha_3 h^{(2)}\right)\right] \\ h^{(4)} &= -\Delta t \delta^B \left[F\left(U^n + \alpha_4 h^{(3)}\right)\right] \\ h^{(5)} &= -\Delta t \delta^F \left[F\left(U^n + \alpha_5 h^{(4)}\right)\right] \\ h^{(6)} &= -\Delta t \delta^B \left[F\left(U^n + \alpha_6 h^{(5)}\right)\right] \\ U^{n+1} &= U^n + \beta_1 h^{(1)} + \beta_2 h^{(2)} + \beta_3 h^{(3)} + \beta_4 h^{(4)} + \beta_5 h^{(5)} + \beta_6 h^{(6)}, \end{aligned} \tag{27}$$

where δ^F refers to a forward spatial difference and δ^B to a backward spatial difference. Normally, the order of forward and backward differences is interchanged every step to avoid numerical biasing.

The coefficients for the three time marching schemes are given in Table II. The RK2 scheme is second-order accurate, while the RK4 and the 4-6 low dispersion and dissipation Runge–Kutta (LDDRK) scheme of Hu *et al.* [13] are both fourth-order accurate in a linear sense. However, for nonlinear problems, the RK4 scheme is fourth-order accurate while the 4-6 LDDRK method presented here reduces to third order accuracy. Notice that the 4-6 LDDRK method uses a two-step marching cycle; one step has four stages and the second step has six.

4. ACCURACY ANALYSIS

Consider a general MacCormack-type method, which is kth order accurate in time. The underlying central difference is lth order accurate in space, while the biased differences are

TABLE II
Time Marching Schemes

	RK2	RK4	LDDRK 4-6 Step 1	LDDRK 4-6 Step 2
α_2	1	1/2	1/2	0.353323
α_3	0	1/2	1/2	0.999597
α_4	0	1	1	0.152188
α_5	0	0	0	0.534216
α_6	0	0	0	0.603907
β_1	1/2	1/6	1/6	0.0467621
β_2	1/2	1/3	1/3	0.137286
β_3	0	1/3	1/3	0.170975
β_4	0	1/6	1/6	0.197572
β_5	0	0	0	0.282263
β_6	0	0	0	0.165142
c_1	1	1	1	1
c_2	1/2	1/2	1/2	1/2
c_3	0	1/6	1/6	1/6
c_4	0	1/24	1/24	1/24
c_5	0	0	0	0.0162098
c_6	0	0	0	0.00286365

mth order accurate in space. A linear accuracy analysis using Eq. (25) will give

$$U(t + \Delta t) = U(t) + \frac{\partial U}{\partial t} + \vartheta(\Delta t^k, \Delta t \Delta x^{m+1}, \Delta x^l). \tag{28}$$

From Eq. (20), the 4/2 scheme will have a third-order time-space error term, while the 4/4 scheme is a true fourth-order method. Using the RK2 time stepping scheme, we find that the 4/2 scheme will be fourth-order accurate in space and second-order accurate in time, even for nonlinear problems, if we alternate the order of the forward and backward sweeps. This result was previously noted in Ref. [2] for the explicit 4/2 scheme of Gottlieb and Turkel. The 4/4 scheme will be fourth-order accurate in space even without alternating the order of the sweeps. For the other time stepping methods, the time accuracy will depend only on the nonlinear accuracy of the time advancement algorithm.

A wavenumber analysis of these schemes gives a more complete picture of their linear performance and stability. The numerical wavenumber $\bar{\theta}\Delta x$ for a general three-point compact derivative (Eq. (13)) is defined as

$$\bar{\theta}\Delta x = \frac{-i(ke^{-i\theta\Delta x} - (k+m) + me^{i\theta\Delta x})}{(ae^{-i\theta\Delta x} + 1 - (a+c) + ce^{i\theta\Delta x})}, \tag{29}$$

where $\theta\Delta x$ is the actual wavenumber and

$$-\pi \le \theta\Delta x \le \pi. \tag{30}$$

For the standard compact scheme, the numerical wavenumber is given by

$$\bar{\theta}\Delta x = \frac{\sin(\theta\Delta x)}{(2/3 + (1/3)\cos(\theta\Delta x))}. \tag{31}$$

Notice that the right side of Eq. (31) is purely real. This is a property of central-difference stencils. For the 4/2 MacCormack-type scheme, the numerical wavenumber for the forward biased difference is

$$\bar{\theta}^F \Delta x = \left(\frac{\sin(\theta \Delta x)}{(2/3 + (1/3)\cos(\theta \Delta x))} - \frac{(i/\sqrt{3})(-1 + \cos(\theta \Delta x))}{(2/3 + (1/3)\cos(\theta \Delta x))} \right). \tag{32}$$

Similarly, the numerical wavenumber for the backward biased difference is

$$\bar{\theta}^B \Delta x = \left(\frac{\sin(\theta \Delta x)}{(2/3 + (1/3)\cos(\theta \Delta x))} + \frac{(i/\sqrt{3})(-1 + \cos(\theta \Delta x))}{(2/3 + (1/3)\cos(\theta \Delta x))} \right). \tag{33}$$

There are two interesting things to observe in Eqs. (32) and (33). First, the real (dispersive) part of both equations is equal and identical to the real part of Eq. (31); thus, the 4/2 scheme has the same dispersion characteristics as a central fourth-order compact scheme. Second, the imaginary (dissipative) parts are equal and opposite. This is a property of MacCormack-type schemes.

Likewise, the numerical wavenumbers for the 4/4 scheme are

$$\bar{\theta}^F \Delta x = \left(\frac{((2/9)\sin(\theta \Delta x) - (1/18)\sin(2\theta \Delta x))}{(5/9 + (4/9)\cos(\theta \Delta x))} - \frac{i(-5/18 + (2/9)\cos(\theta \Delta x) + (1/18)\cos(2\theta \Delta x))}{(5/9 + (4/9)\cos(\theta \Delta x))} \right) \tag{34}$$

$$\bar{\theta}^B \Delta x = \left(\frac{((2/9)\sin(\theta \Delta x) - (1/18)\sin(2\theta \Delta x))}{(5/9 + (4/9)\cos(\theta \Delta x))} + \frac{i(-5/18 + (2/9)\cos(\theta \Delta x) + (1/18)\cos(2\theta \Delta x))}{(5/9 + (4/9)\cos(\theta \Delta x))} \right). \tag{35}$$

Figures 1 and 2 show the dispersion properties of these schemes and compare them to explicit schemes such as 4th and 6th order central differences and the 7-point DRP scheme of Tam and Webb [5]. Notice the reduction in the dispersion error throughout the wavenumber range from the 4/4 scheme as compared to the 4/2 scheme; this is due to the change in the underlying central difference in the 4/4 scheme.

In Fig. 2, the DRP scheme and 4/4 scheme both exhibit "dips" in the dispersion error curve. The reason for this is illustrated in Fig. 1. Notice that the numerical wavenumber of the 4/4 scheme is greater than the actual wavenumber through a large portion of the wavenumber spectrum, dipping below at a wavenumber value of about 2.6. When the numerical wavenumber crosses through the actual wavenumber, they are equal and the error is zero, causing the "dip" in Fig. 2. The DRP scheme also has a numerical wavenumber that is greater than the actual wavenumber at low wavenumbers; at the scale of Fig. 1 it cannot be seen.

Figure 3 shows the dissipation properties of the two MacCormack-type schemes. Again, the reduction in dissipation in the resolved wavenumber range from the 4/4 scheme is evident.

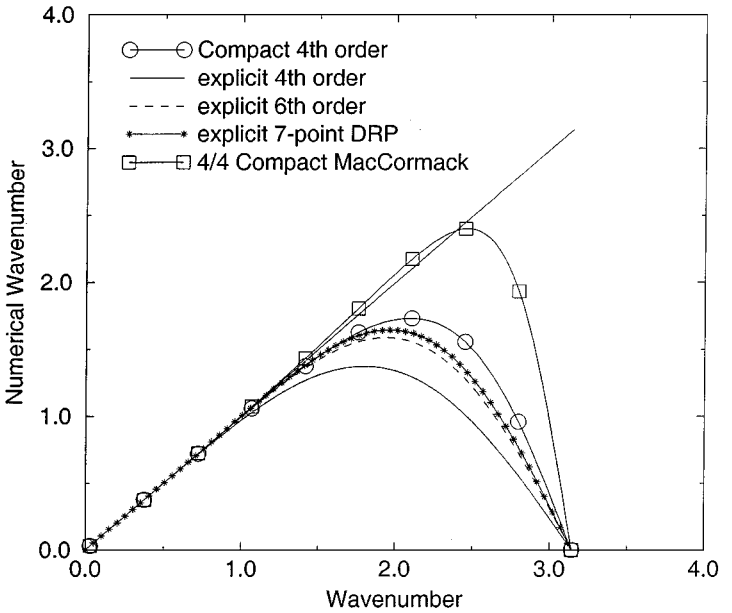

FIG. 1. Dispersion characteristics of compact MacCormack-type schemes.

5. PERFORMANCE AND STABILITY OF COMPACT MACCORMACK-TYPE SCHEMES

The numerical wavenumber of the forward and backward operators of a MacCormack-type scheme may be written as

$$\begin{aligned} \overline{\theta}^F \Delta x &= \overline{\theta}^C \Delta x - i(\delta \Delta x) \\ \overline{\theta}^B \Delta x &= \overline{\theta}^C \Delta x + i(\delta \Delta x). \end{aligned} \tag{36}$$

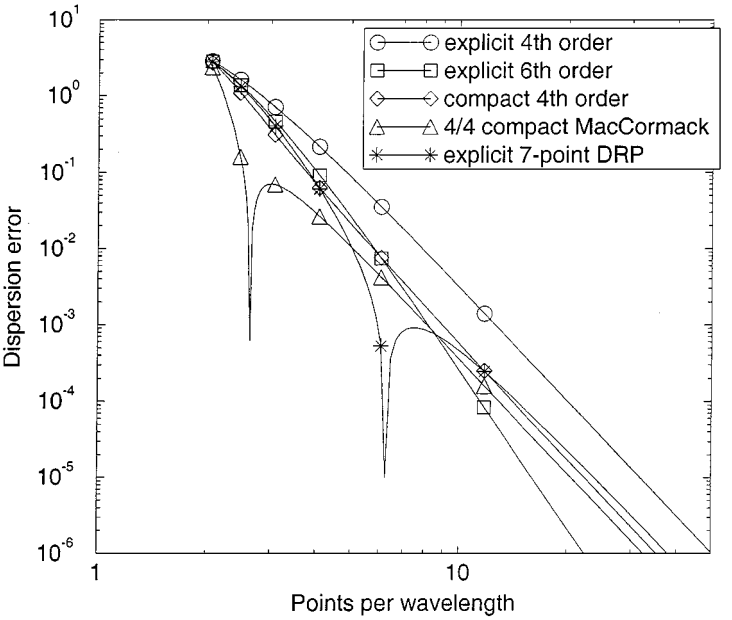

FIG. 2. Dispersion error magnitude comparison.

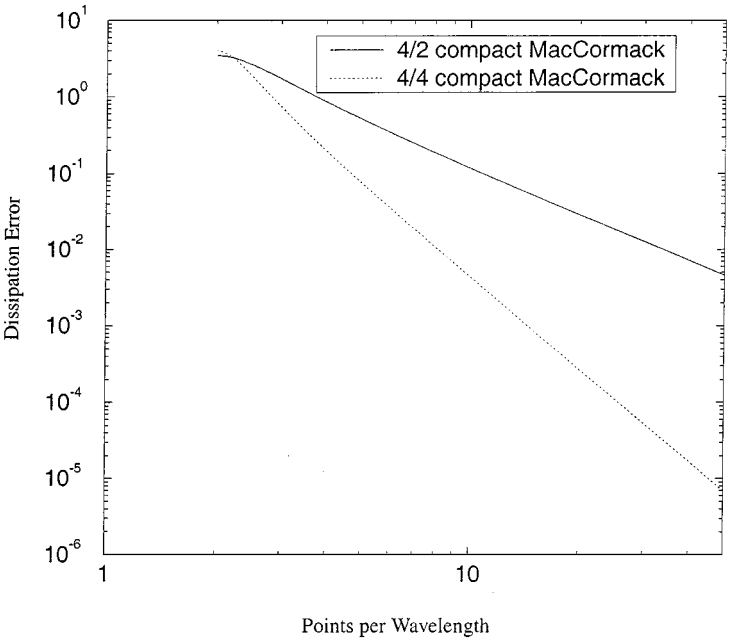

FIG. 3. Dissipation magnitude for compact MacCormack-type schemes.

As previously noted, the dispersion relation $\bar{\theta}^C \Delta x$ is the same for both the forward and backward differences; however, the dissipative term $\delta \Delta x$ is equal and opposite.

Substituting these definitions into the time-marching schemes described above, we obtain

$$\begin{aligned} U(t+\Delta t) = (1 &+ c_1(-i\Delta t)(\bar{\theta}^C \Delta x) + c_2(-i\Delta t)^2((\bar{\theta}^C \Delta x)^2 + (\delta \Delta x)^2) \\ &+ c_3(-i\Delta t)^3(\bar{\theta}^C \Delta x)((\bar{\theta}^C \Delta x)^2 + (\delta \Delta x)^2) + c_4(-i\Delta t)^4((\bar{\theta}^C \Delta x)^2 \\ &+ (\delta \Delta x)^2)^2 + c_5(-i\Delta t)^5(\bar{\theta}^C \Delta x)((\bar{\theta}^C \Delta x)^2 + (\delta \Delta x)^2)^2 \\ &+ c_6(-i\Delta t)^6((\bar{\theta}^C \Delta x)^2 + (\delta \Delta x)^2)^3)U(t) = \langle G(\theta \Delta x) \rangle U(t). \end{aligned} \tag{37}$$

Using this equation, we can find the linear wavenumber response of the time-marching scheme, as well as its linear stability. For this stability analysis, the magnitude of $G(\theta \Delta x)$ must be equal to or less than one for $0 < \theta \Delta x < \pi$. In this work, $\theta \Delta x \to 0$ and $\theta \Delta x = \pi$, which measure the long and short wavelength stability, are investigated analytically. As a matter of observation, if the scheme is stable for small $\theta \Delta x$ and for $\theta \Delta x = \pi$, it is almost always stable for all $\theta \Delta x$.

Table III shows the results for the linear stability analysis, both analytical and numerical.

6. BOUNDARY STENCILS FOR COMPACT MACCORMACK-TYPE SCHEMES

6.1. Effect of boundary stencils on interior scheme performance. The numerical properties of the boundary stencil for a compact scheme has a much larger effect on the stability

TABLE III
Stability Limits

Scheme	Time marching	CFL limit ($\theta\Delta x \to 0$)	CFL limit ($\theta\Delta x \to \pi$)	CFL limit (numerical)
4/2	RK2	$\frac{1}{\sqrt{3}}$	$\frac{1}{\sqrt{3}}$	0.577
	RK4	(stable)	1	1.0
	LDDRK 4-6	(stable)	0.934684	0.891
4/4	RK2	(unstable)	$\frac{1}{2}$	(unstable)
	RK4	(stable)	$\frac{\sqrt{3}}{2}$	0.851
	LDDRK 4-6	(stable)	0.80946	0.747

and accuracy of the scheme than the boundary stencil for the equivalent explicit scheme [15, 16]. The reason for this is that the error from the boundary stencil can propagate many points into the computational domain.

Taking the 4/2 scheme as an example, let us assume that we have an error ε_0 from the boundary at the beginning of the backward sweep. Define ε_0 as

$$\varepsilon_0 = (D^B)_{interior} - (D^B)_{boundary}, \tag{38}$$

where the subscript "interior" refers to the spatial derivative that the interior scheme would have obtained and the subscript "boundary" refers to the derivative obtained by the boundary stencil. It can be seen that we are defining the error with respect to the numerical derivative that the interior scheme would have obtained rather than the exact analytical derivative at the boundary.

Substituting (38) into Eq. (19), we find that the error propagates inward from the boundary. The error for a derivative i grid points away from the boundary is

$$(D^B)_{interior}\big|_i = (D^B)_{boundary}\big|_i + \left(-\frac{a}{1-a}\right)^i \varepsilon_0 \tag{39}$$

or

$$\varepsilon_i = \left(-\frac{a}{1-a}\right)^i \varepsilon_0. \tag{40}$$

It is clear that the error due to the boundary stencil used at the start of the sweep has a much greater effect on the computed derivative than that of the boundary stencil used at the end of the sweep. Figure 4 illustrates the effect of boundary stencil error on the interior derivatives for the 4/2 and 4/4 schemes. The 4/2 scheme is less affected by boundary stencil error than the 4/4 scheme.

6.2. Boundary stencil description. One-sided, five-point, explicit boundary stencils were used for the two schemes described. These stencils were obtained by matching the

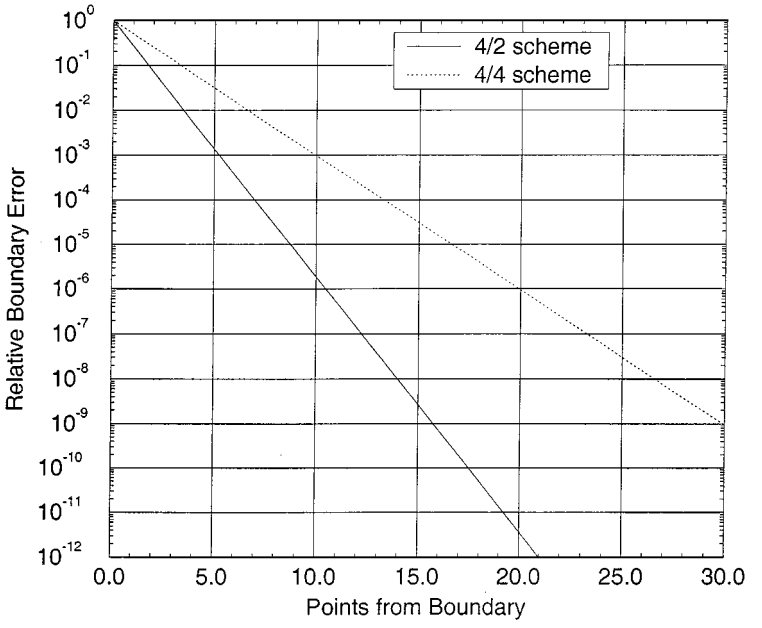

FIG. 4. Effect of boundary stencil error on interior solution.

Taylor series terms to the fourth order for the forward and backward stencils of each scheme. For the 4/2 scheme, the boundary stencils are

$$
\begin{aligned}
D^F_{i\,min} &= \left(-\frac{25}{12}+\frac{17}{12\sqrt{3}}\right) f_i + \left(4-\frac{25}{6\sqrt{3}}\right) f_{i+1} - \left(3-\frac{3\sqrt{3}}{2}\right) f_{i+2} \\
&\quad + \left(\frac{4}{3}-\frac{13}{6\sqrt{3}}\right) f_{i+3} - \left(\frac{1}{4}-\frac{5}{12\sqrt{3}}\right) f_{i+4} \\
D^B_{i\,min} &= -\left(\frac{25}{12}+\frac{17}{12\sqrt{3}}\right) f_i + \left(4+\frac{25}{6\sqrt{3}}\right) f_{i+1} - \left(3+\frac{3\sqrt{3}}{2}\right) f_{i+2} \\
&\quad + \left(\frac{4}{3}+\frac{13}{6\sqrt{3}}\right) f_{i+3} - \left(\frac{1}{4}+\frac{5}{12\sqrt{3}}\right) f_{i+4} \\
D^F_{i\,max} &= \left(\frac{25}{12}+\frac{17}{12\sqrt{3}}\right) f_i - \left(4+\frac{25}{6\sqrt{3}}\right) f_{i-1} + \left(3+\frac{3\sqrt{3}}{2}\right) f_{i-2} \\
&\quad - \left(\frac{4}{3}+\frac{13}{6\sqrt{3}}\right) f_{i-3} + \left(\frac{1}{4}+\frac{5}{12\sqrt{3}}\right) f_{i-4} \\
D^B_{i\,max} &= \left(\frac{25}{12}-\frac{17}{12\sqrt{3}}\right) f_i - \left(4-\frac{25}{6\sqrt{3}}\right) f_{i-1} + \left(3-\frac{3\sqrt{3}}{2}\right) f_{i-2} \\
&\quad - \left(\frac{4}{3}-\frac{13}{6\sqrt{3}}\right) f_{i-3} + \left(\frac{1}{4}-\frac{5}{12\sqrt{3}}\right) f_{i-4}.
\end{aligned}
\tag{41}
$$

For the 4/4 scheme, the boundary stencils used were

$$
\begin{aligned}
D^F_{i\,min} &= \left(-\frac{19}{9}\right) f_i + \left(\frac{37}{9}\right) f_{i+1} - \left(\frac{19}{6}\right) f_{i+2} + \left(\frac{13}{9}\right) f_{i+3} - \left(\frac{5}{18}\right) f_{i+4} \\
D^B_{i\,min} &= -\left(\frac{37}{18}\right) f_i + \left(\frac{35}{9}\right) f_{i+1} - \left(\frac{17}{6}\right) f_{i+2} + \left(\frac{11}{9}\right) f_{i+3} - \left(\frac{2}{9}\right) f_{i+4} \\
D^F_{i\,max} &= \left(\frac{37}{18}\right) f_i - \left(\frac{35}{9}\right) f_{i-1} + \left(\frac{17}{6}\right) f_{i-2} - \left(\frac{11}{9}\right) f_{i-3} + \left(\frac{2}{9}\right) f_{i-4} \\
D^B_{i\,max} &= \left(\frac{19}{9}\right) f_i - \left(\frac{37}{9}\right) f_{i-1} + \left(\frac{19}{6}\right) f_{i-2} - \left(\frac{13}{9}\right) f_{i-3} + \left(\frac{5}{18}\right) f_{i-4}.
\end{aligned}
\tag{42}
$$

This is not the only option for boundary stencil specification. Another possibility is to define ghost points outside the computational domain and extrapolate data to these artificial points using high-order accurate extrapolation. In this way, the interior scheme can be used on the boundaries (see, e.g., Ref. [3]). For the fourth-order accurate compact schemes given here, only one ghost point is needed.

7. BENCHMARK TEST PROBLEMS AND RESULTS

Three test problems were chosen to investigate the numerical performance of the two compact MacCormack-type schemes. These problems are from the First and Second CAA Workshops [17–18].

7.1. The 1-D linear wave propagation. The first problem tested is the first linear problem given in the First CAA Workshop [17]. The problem asks for the solution of the 1-D linear convection equation at time = 400,

$$
\begin{aligned}
&U_t + U_x = 0 \\
&U(x, 0) = \frac{1}{2} \exp\left(-\ln(2)\left(\frac{x}{3}\right)^2\right),
\end{aligned}
\tag{43}
$$

where

$$
\Delta x = 1.0 \qquad -20 \le x \le 450. \tag{44}
$$

Boundary condition specification is straightforward in this problem. At $x = -20$, which is the inflow boundary, the derivative of U is set to zero. At $x = 450$, which is the outflow boundary, the derivative of U is calculated explicitly from the interior using one-sided boundary stencils.

Figures 5–7 show the results for the 4/2 scheme used with each time-stepping method at varying time steps. As noted in Ref. [9], the RK2 time-stepping method shows a tendency to affect the dispersion as the time step increases, while the RK4 method tends to be dissipative at higher time steps. The LDDRK 4-6 method also dissipates at higher time steps when combined with the 4/2 scheme; however, this is more due to the scheme itself than the time stepping method.

Figure 8 shows the results for the 4/4 method at a time step of CFL = 0.5 for both the RK4 and LDDRK 4-6 time stepping methods. Due to the specification of the problem

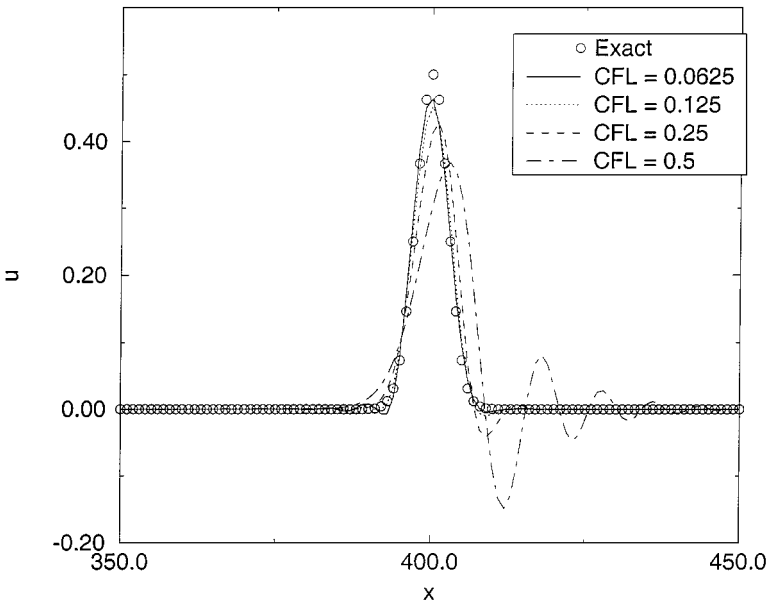

FIG. 5. Performance of 4/2 scheme using RK2 time marching on benchmark problem 1.

and the stability limits of the schemes, this was the largest time step that could be used. The improvement in dissipation and dispersion from the 4/4 scheme is evident, though the difference between the two time marching methods is small at this low time step. As the time step is increased, the LDDRK 4-6 method will show an improvement over the RK4 method, as noted in Refs. [9, 10].

7.2. The 1-D shock tube problem. The second one-dimensional problem solves the Category 2 shock tube problem from the First CAA Workshop [17]. The equations solved

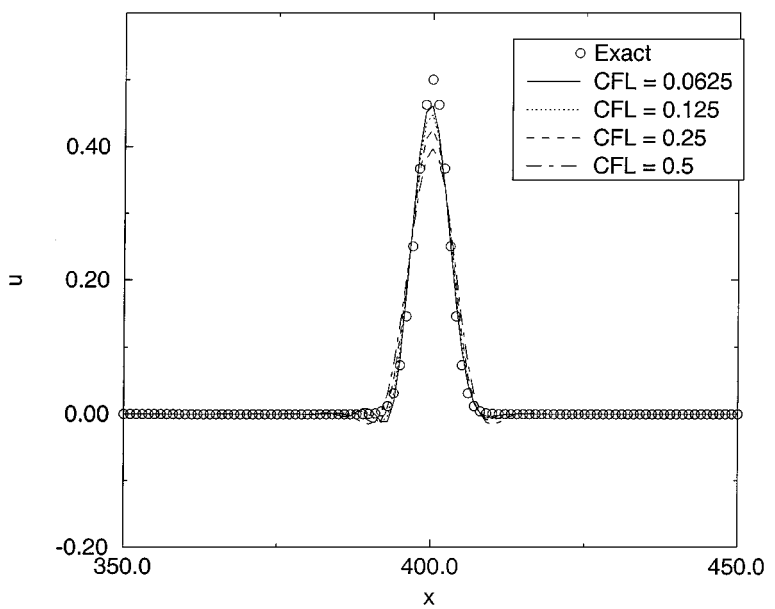

FIG. 6. Performance of 4/2 scheme using RK4 time marching on benchmark problem 1.

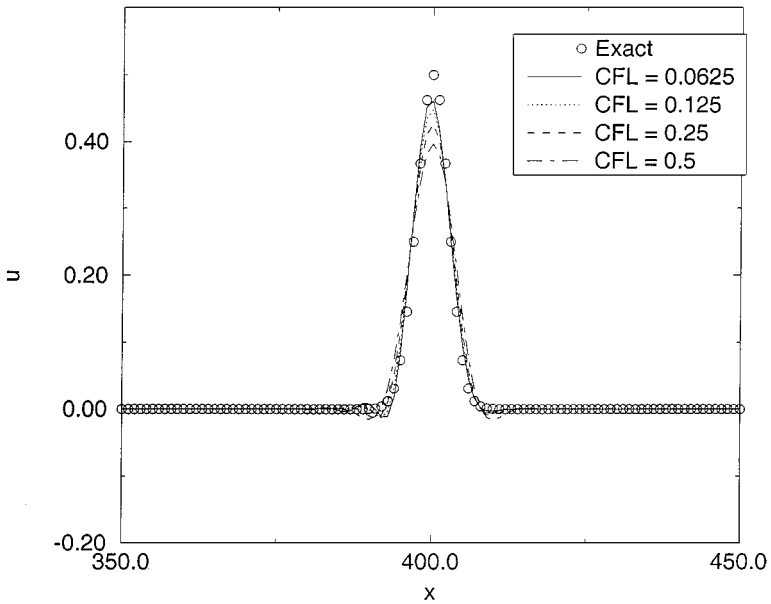

FIG. 7. Performance of 4/2 scheme using LDDRK 4-6 time marching on benchmark problem 1.

are the nonlinear Euler equations, written in conservative form,

$$\frac{d}{dt}\begin{Bmatrix}\rho\\ \rho u\\ E\end{Bmatrix}+\frac{d}{dx}\begin{Bmatrix}\rho u\\ \rho u^2+p\\ u(E+p)\end{Bmatrix}=0, \tag{45}$$

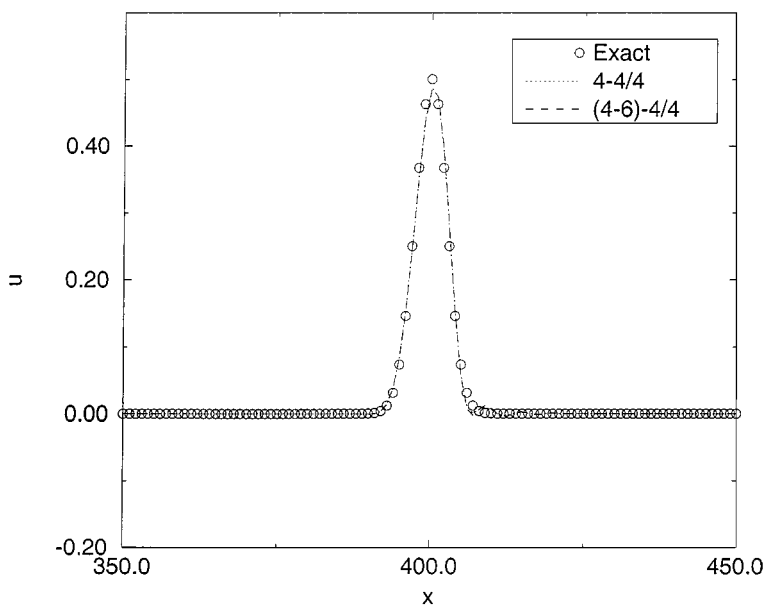

FIG. 8. Performance of 4/4 scheme on benchmark problem 1.

where

$$p = (\gamma - 1)\left(E - \frac{1}{2}\rho u^2\right). \tag{46}$$

The equations are solved on the domain $-100 < x < 100$, with $\Delta x = 1.0$. The initial conditions are

$$\begin{aligned} u(x,0) &= 0 \\ p(x,0) &= \begin{cases} 4.4, & x < -2 \\ 2.7 + 1.7\cos\left(\frac{(x+2)\pi}{4}\right), & -2 < x < 2 \\ 1.0, & x > 2 \end{cases} \\ \rho(x,0) &= (\gamma p)^{1/\gamma}. \end{aligned} \tag{47}$$

The boundary conditions used are the one-dimensional characteristic formulation. The three characteristics are given by

$$\begin{aligned} c_1 &= \frac{dp}{dt} - \bar{\rho}\bar{c}\frac{du}{dt} \\ c_2 &= \bar{c}^2\frac{d}{dt}(\rho) - \frac{dp}{dt} \\ c_3 &= \frac{dp}{dt} + \bar{\rho}\bar{c}\frac{du}{dt}, \end{aligned} \tag{48}$$

where the overbar terms are mean values that are set in this work as the initial values at the boundary. In this formulation, outgoing characteristics are computed using the interior scheme, while incoming characteristics are set to zero. For the inflow boundary ($x = -100$), c_1 and c_2 are incoming and are set to zero. For the outflow boundary ($x = 100$), c_3 is incoming and is set to zero.

Figures 9 and 10 show the results for density at time = 60 for this problem compared to the exact solution. In these figures, the expansion fan is shown on the left, with the contact surface in the middle and the shock on the right. Only part of the computational domain is shown in order to illustrate the performance of the different methods.

In Fig. 9, the three time stepping methods are compared using the 4/2 scheme. All three use a time step of CFL = 0.25. This figure shows the ability of all three methods to accurately track the discontinuities, with the RK2 time stepping method having more oscillations in the solution than the other two methods.

In Fig. 10, the 4/4 scheme is tested using the RK4 and LDDRK 4-6 time stepping methods. At this small time step, both methods produce comparable results. Notice that while the 4/4 method does have more oscillations in the solution compared to the 4/2 method, the contact surface is more sharply resolved. This is due to the decreased dissipation and increased dispersion accuracy of the 4/4 method.

For all cases, the solution of the shock tube problem could be improved by using artificial dissipation or filtering to damp the numerical oscillations. However, the results show that the schemes are all stable in the vicinity of a discontinuity without additional damping.

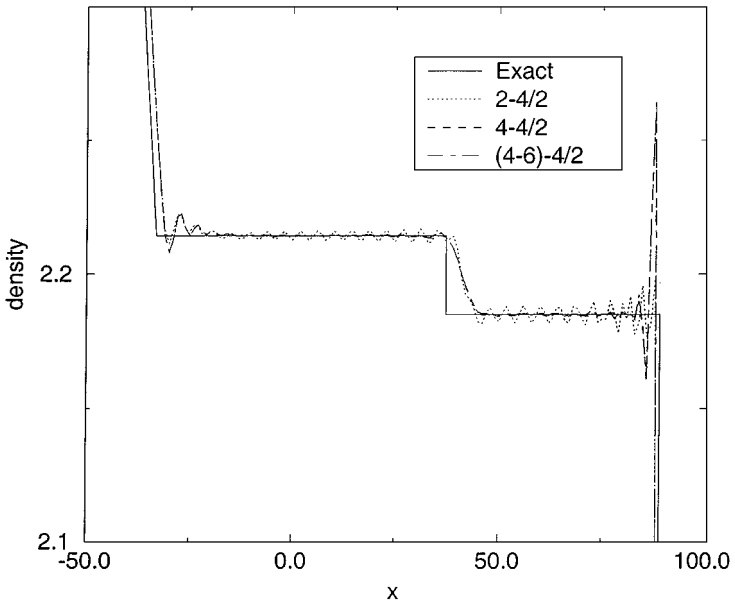

FIG. 9. Effect of time stepping method on 4/2 scheme solution of nonlinear benchmark problem 2 (CFL = 0.25).

7.3. The 2-D acoustic scattering problem. The third test problem is from the Second CAA Workshop [18]. In this problem, a 2-D cylinder of radius $R = 0.5$ is located at the origin. At time = 0, an initial pressure pulse is specified:

$$p(x, y, 0) = \exp\left(-\ln(2)\left(\frac{(x-4)^2 + y^2}{0.04}\right)\right). \tag{49}$$

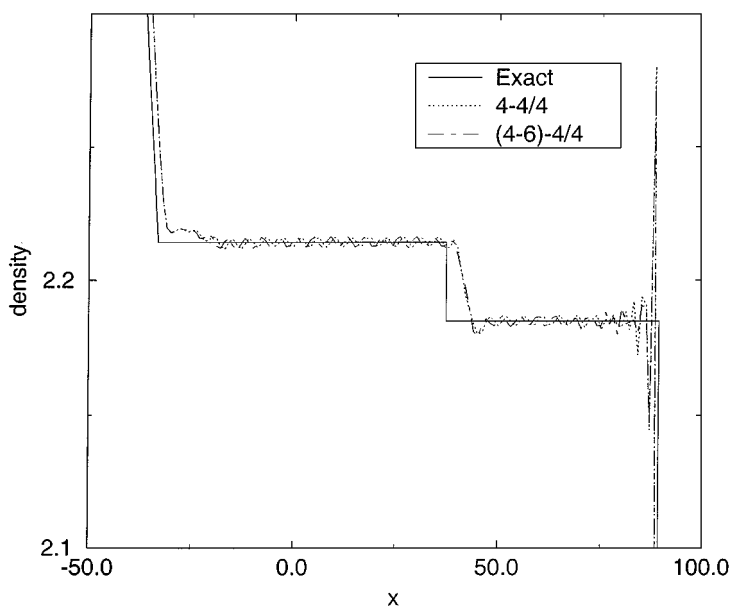

FIG. 10. Effect of time stepping method on 4/4 scheme solution of nonlinear benchmark problem 2 (CFL = 0.25).

The problem asks for the unsteady pressure data for $6 < t < 10$ at three stations: $(0, 5)$, $(5/\sqrt{2}, 5/\sqrt{2})$, and $(-5, 0)$.

The equations to be solved are the linearized Euler equations in polar coordinates:

$$\frac{d}{dt}\begin{Bmatrix} v_r \\ v_\theta \\ p \end{Bmatrix} + \frac{d}{dr}\begin{Bmatrix} p \\ 0 \\ v_r \end{Bmatrix} + \frac{1}{r}\frac{d}{d\theta}\begin{Bmatrix} 0 \\ p \\ v_\theta \end{Bmatrix} = \frac{1}{r}\begin{Bmatrix} 0 \\ 0 \\ v_r \end{Bmatrix}. \tag{50}$$

The computational domain extends radially from $R = 0.5$ to $R = 10.5$, and azimuthally from $\theta = 0$ to $\theta = 2\pi$. Three boundary conditions are used: a wall condition on the cylinder, an acoustic radiation condition in the far field, and a periodic condition at the azimuthal boundaries.

The wall condition is based on the wall condition of Tam and Dong [19]. This condition requires that the time rate of change of the normal velocity at the wall is zero:

$$\frac{dv_r}{dt} = -\frac{dp}{dr} = 0. \tag{51}$$

This condition is imposed by setting the normal derivative of pressure at the wall to zero for each sweep, while the other radial derivatives are computed normally.

The acoustic radiation boundary condition is given by Bayliss and Turkel [20, 21] as

$$\frac{d}{dt}\begin{Bmatrix} v_r \\ v_\theta \\ p \end{Bmatrix} + \frac{d}{dr}\begin{Bmatrix} v_r \\ 0 \\ p \end{Bmatrix} + \frac{1}{2r}\begin{Bmatrix} v_r \\ 0 \\ p \end{Bmatrix} = 0. \tag{52}$$

The radial derivatives at the exterior boundary are computed using one-sided explicit stencils.

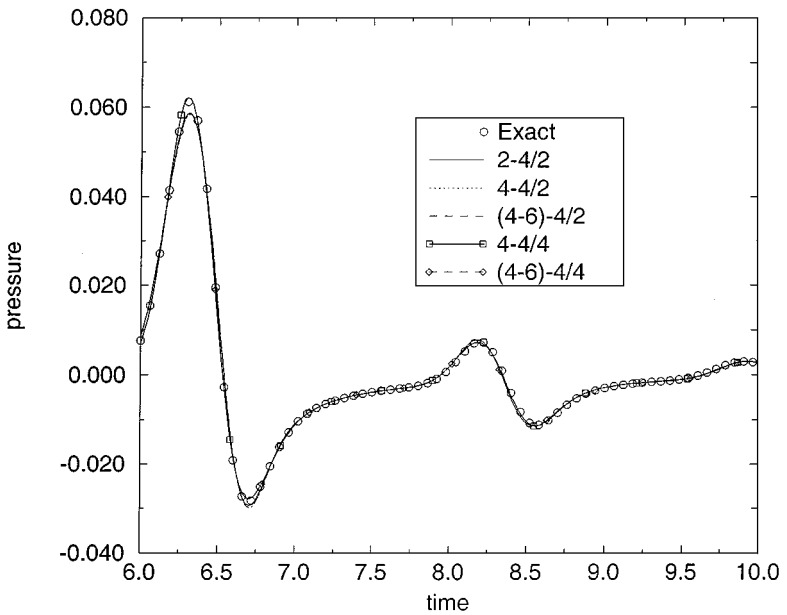

FIG. 11. Solution of benchmark problem 3 at point (0, 5) (CFL = 0.5).

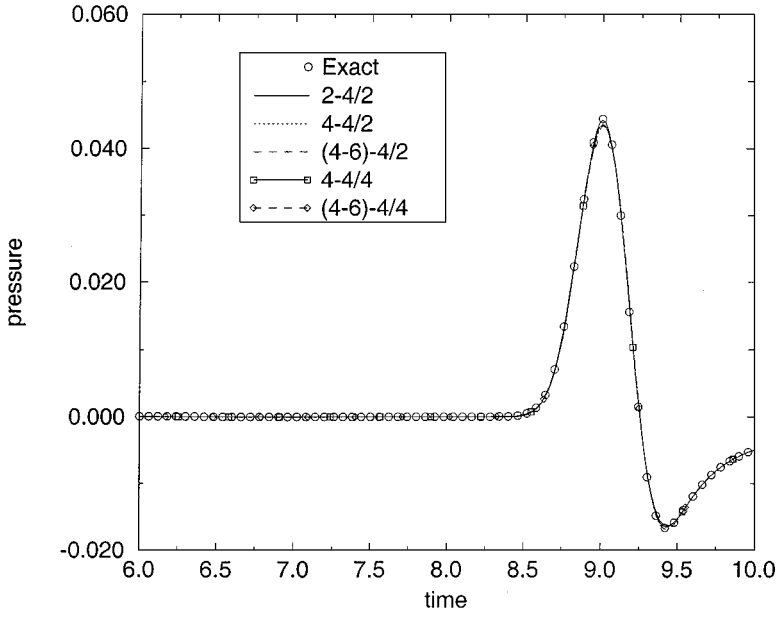

FIG. 12. Solution of benchmark problem 3 at point $(-5, 0)$ (CFL $= 0.5$).

The periodic boundary condition requires some extra work. To start the sweep for the azimuthal derivative, the one-sided boundary stencil is used. At the end of the sweep, a corrected value for the derivative is known, and Eq. (40) is used to update the interior points as required.

For this calculation, a uniformly spaced grid of 201 radial points and 301 azimuthal points is used, with a time step of CFL $= 0.5$. Since the grid does not have a point at $(5/\sqrt{2}, 5/\sqrt{2})$, data are only taken at the points $(0, 5)$ and $(-5, 0)$.

Figures 11 and 12 show the results for these locations, compared to the exact solution. The results of both methods are good for this problem. At the initial transient in Fig. 11, it can be seen that the 4/4 scheme is less dissipative, but has the wave arriving slightly early. The 4/2 scheme is more dissipative, with a lagging dispersion error. At this relatively small time step, all time marching methods perform well.

8. CONCLUSIONS

A new series of compact MacCormack-type schemes are presented which feature one-sided implicit stencils, reducing the computational effort greatly. Explicit boundary stencils and boundary conditions are described, and results are shown for linear and nonlinear CAA benchmark problems. Linear stability and wave propagation properties are shown for the two schemes, using various time-stepping methods. The compact methodology gives a distinct performance advantage over previous explicit MacCormack-type schemes and can be easily added to existing MacCormack scheme solvers.

ACKNOWLEDGMENTS

This work was carried out under Grant NCC3-531 from the NASA Glenn Research Center while the first author was in residence at the Institute for Computational Mechanics in Propulsion at the Ohio Aerospace Institute. Dr. L. A. Povinelli was the Technical Monitor.

REFERENCES

1. H. O. Kreiss, S. A. Orszag, and M. Israeli, *Ann. Rev. Fluid Mech.* **6**, 281 (1974).
2. D. Gottlieb and E. Turkel, Dissipative two-four method for time dependent problems, *Math. Comput.* **30**, 703 (1976).
3. A. Bayliss, L. Maestrello, P. Parikh, and E. Turkel, *A Fourth-Order Method for the Unsteady Compressible Navier–Stokes Equations*, AIAA Paper 85-1694, 1985.
4. S. K. Lele, Compact finite difference schemes with spectral-like resolution, *J. Comput. Phys.* **103**, 16 (1992).
5. C. K. W. Tam and J. C. Webb, Dispersion-relation-preserving finite difference schemes for computational acoustics, *J. Comput. Phys.* **107**, 262 (1993).
6. D. W. Zingg, H. Lomax, and H. M. Jurgens, *An Optimized Finite-Difference Scheme for Wave Propagation Problems*, AIAA Paper 93-0459, AIAA 30th Aerospace Sciences Meeting and Exhibit, Reno, Nevada, 1993 (unpublished).
7. Z. Haras and S. Ta'asan, Finite-difference schemes for long-time integration, *J. Comput. Phys.* **114**, 265 (1994).
8. C. A. Kennedy and M. H. Carpenter, Several new numerical methods for compressible shear-layer simulations, *Appl. Numer. Math.* **14**, 397 (1994).
9. R. Hixon, *On Increasing the Accuracy of MacCormack Schemes for Aeroacoustic Applications*, AIAA Paper 97-1586, 3rd AIAA/CEAS Aeroacoustics Conference, Atlanta, GA, 1997 (unpublished).
10. R. Hixon, Evaluation of a high-accuracy MacCormack-type scheme using benchmark problems. *J. Comput. Acoustics* **6**, 291 (1998).
11. R. Hixon, *A New Class of Compact Schemes*, AIAA Paper 98-0367, AIAA 35th Aerospace Sciences Meeting and Exhibit, Reno, Nevada, 1998 (unpublished).
12. R. Hixon, *Prefactored Compact Filters for Computational Aeroacoustics*, AIAA Paper 99-0358, AIAA 36th Aerospace Sciences Meeting and Exhibit, Reno, NV, 1999 (unpublished).
13. F. Q. Hu, M. Y. Hussaini, and J. Manthey, Low-dissipation and dispersion Runge–Kutta schemes for computational acoustics, *J. Comput. Phys.* **124**, 121 (1996).
14. M. H. Carpenter, D. Gottlieb, and S. Abarbanel, Stable and accurate boundary treatments for compact, high-order finite-difference schemes, *Appl. Numer. Math.* **12**, 55 (1993).
15. M. H. Carpenter, D. Gottlieb, and S. Abarbanel, Time-stable boundary conditions for finite-difference schemes solving hyperbolic systems: Methodology and application to high-order compact schemes, *J. Comput. Phys.* **111**, 220 (1994).
16. C. K. W. Tam, Benchmark problems, in *ICASE/LaRC Workshop on Benchmark Problems in Computational Aeroacoustics* (NASA CP-3300, Hampton, VA, 1995), p. 1.
17. C. K. W. Tam and J. C. Hardin (Eds.), *Second Computational Aeroacoustics (CAA) Workshop on Benchmark Problems* (NASA CP-3352, Hampton, VA, 1997), p. 1.
18. C. K. W. Tam and Z. Dong, Wall boundary conditions for high-order finite difference schemes in computational aeroacoustics, *Theoret. Comput. Fluid Dynam.* **6**, 303 (1994).
19. A. Bayliss and E. Turkel, Radiation boundary conditions for wave-like equations, *Comm. Pure Appl. Math.* **33**, 707 (1980).
20. A. Bayliss and E. Turkel, Far field boundary conditions for wave-like equations, *J. Comput. Phys.* **48**, 182 (1982).